Inorganic Chemistry

Article

pubs.acs.org/IC

Structural, Spectral, and Electrochemical Properties of Nickel(II), Copper(II), and Zinc(II) Complexes Containing 12-Membered Pyridine- and Pyridol-Based Tetra-aza Macrocycles

Kimberly M. Lincoln, Michael E. Offutt, Travis D. Hayden, Ryker E. Saunders, and Kayla N. Green*

Department of Chemistry, Texas Christian University, Fort Worth, Texas 76109, United States

Supporting Information

ABSTRACT: The structural, electronic, and electrochemical properties of a series of novel 12-membered pyridine- and pyridol-based tetra-aza transition-metal (Ni, Cu, Zn) complexes {$[M^{II}(\mathbf{L1})Cl](ClO_4)$, $[M^{II}(\mathbf{L2})Cl](ClO_4)$, and $[M^{II}(\mathbf{L3})Cl](ClO_4)$} are described (**L1** (Pyclen) = 1,4,7,10-tetra-aza-2,6-pyridinophane; **L2** = 3,6,9,15-tetraazabicyclo[9.3.1]penta-deca-1(15),11,13-trien-13-ol; **L3** = 3,6,9,15-tetra-azabicyclo[9.3.1]penta-deca- 1(15),11,13-trien-12-ol). The subtle variations in the chemical properties of these complexes were investigated using X-ray crystallography, UV−vis and NMR spectroscopy, and cyclic voltammetry. In the solid-state, the Ni(II) complexes adopt a unique bimetallic and *cis*-octahedral $(\mu\text{-Cl})_2$ coordination sphere, and the electronic studies provide further evidence for the existence of a six-coordinate Ni(II) species in solution. The pyridol-based Cu(II) and Zn(II) complexes contain five-coordinate (N_4Cl) geometries in the solid-state, in which the four N-donor atoms are not coplanar. Hydroxylation of the pyridine ring was found to increase the amount of π electronic charge density residing throughout the aromatic system of the ligand backbone, increase the strength of the M−Cl and M−N (pyridine) basal *x*- and *y*-plane interactions, and decrease the axial M−N bonding interaction. The electrochemical studies demonstrate that (i) the Lewis-acidity of the metal center systematically decreases across the series {$[Cu^{II}(\mathbf{L3})Cl](ClO_4)$ > $[Cu^{II}(\mathbf{L1})Cl](ClO_4)$ > $[Cu^{II}(\mathbf{L2})Cl](ClO_4)$}, and (ii) the aromatic backbones allow access to both Cu(I) and Cu(III) species in solution. Overall, the experimental findings are consistent with the idea that *p*-hydroxylation enhances the Lewis-basicity of pyridine-based macrocycle and decreases the Lewis-acidity of the metal-ion, while *m*-hydroxylation decreases the electron-donating ability of the backbone and increases the metal-ion Lewis-acidity.

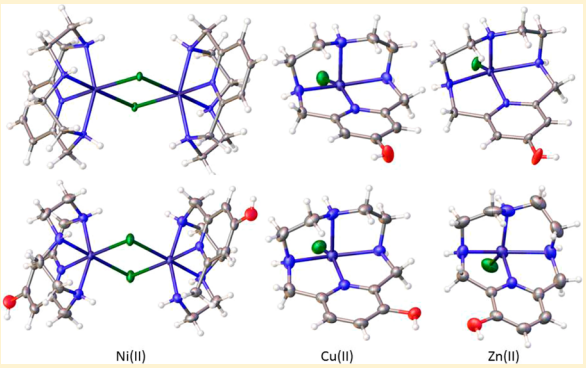

INTRODUCTION

Tetra-aza macrocycles represent a unique family of ligands that are utilized across a wide variety of fields, stemming from the ability to form stable complexes with a wide range of both transition and lanthanide metal cations.[1−10] The versatile reactivity displayed by these molecules is fundamentally attributed to the promiscuous metal-binding nature of the cyclic tetra-aza backbone.[15] The specific function for which a particular complex may play a role is largely dependent upon the species of metal bound and whether or not the metal center is redox active.[2−4,7−18] Factors such as the cavity size,[2,15,19−24] denticity,[3−6,8−10] flexibility,[2,18,21,22,25,26] and the presence of substituents[2,10,13,14,21,27−29] are *all* important structural elements which deeply influence the geometry of the metal coordination sphere and corresponding redox activity of the metal center. Tetra-aza macrocycles have a strong preference to coordinate 3d transition metal-ions in a coplanar manner, where the strength of the in-plane metal−nitrogen interactions is modulated according the size of the ligand cavity.[2,15,19,20,23,28,29]

Bush and Fabbrizzi have each established that size of the fully saturated 14-membered cyclam cavity is an ideal host for coordination of the first-row divalent transition metal-ions because the cavity size is spacious enough to allow coplanar (N_4) coordination between the ligand and metal-ion.[15,20] Accordingly, ligands derived from smaller 12- and 13-membered cavities restrict the coplanar coordination of the metal-ion, forcing the ligand backbone to adopt a cis-folded geometric arrangement where the metal-ion lies outside of the N_4 plane.[11,18,19,22,24] The folding of the ligand backbone induces ring strain throughout the structural framework of the macrocycle, consequentially promoting distorted square-pyramidal, trigonal-bipyramidal, or pseudo-octahedral geometric arrangements about the metal center.[3,4,7,15,18,19,23,24] The deviation of the macrocyclic ligand from planarity significantly affects the electrochemical properties of the complexes and leads to the stabilization of rather uncommon metal oxidation states, and this behavior is well-documented.[2,4,7,18,19,21,23,28] Transition metal complexes derived from tetra-aza ligands, for example, tend to display rather unusual redox behavior. Oxidation states such as Ni(I)/Ni(III)

Received: September 5, 2013
Published: January 17, 2014

 © 2014 American Chemical Society dx.doi.org/10.1021/ic402119s | *Inorg. Chem.* 2014, 53, 1406−1416

and Cu(I)/Cu(III) are often produced easily within the tetra-aza core, and the stability of these valence states can be tuned according to the structure of the ligand backbone.[2,13,14,16−18,20−23,25,26,28−30] Electrochemical studies conducted on pyridine-based tetra-aza complexes containing Fe and Cu are noteworthy and have been recognized in the fields of biomimetic and organometallic catalysis, respectively.[13,14,17,18] Lastly, investigations concerning the redox-structure relationship between the macrocyclic ligand and metal-ion have established that the incorporation of unsaturation into the structure of the tetra-aza backbone is necessary for the stabilization of low-valence transition metal species in solution.[20,21,26,28] For instance, complexes derived from Schiff-base and pyridine-based backbones permit the electrochemical formation of stable Ni(I) and Cu(I) species in solution.[16,25,26,28]

Chemical interest in our research group is largely centered on the 12-membered pyridine- and pyridol-based tetra-aza macrocycles **L1**−**L3** (Figure 1) (**L1** (Pyclen) = 1,4,7,10-tetra-aza-2,6-pyridinophane; **L2** = 3,6,9,15-tetraazabicyclo[9.3.1]-penta-deca-1(15),11,13-trien-13-ol; **L3** = 3,6,9,15-tetra-azabicyclo[9.3.1]penta-deca-1(15),11,13-trien-12-ol). Initial studies were focused on the use of the free macrocycles as therapeutic compounds aimed specifically toward neuro-degenerative disorders characterized by Cu-ion misregulation, in conjunction with oxidative stress. Previously, we reported that the macrocycles **L1** and **L2** are capable of both disrupting and preventing the Cu(II)-induced formation of beta-amyloid plaques in vitro.[31,32] In addition, the N-heterocyclic backbones possess antioxidant and radical scavenging properties and demonstrate the ability to protect cells (Friedreich's ataxia fibroblasts) against death induced by reactive oxygen species. Notably, the *p*-hydroxyl substituted ligand (**L2**) displays a superior antioxidant and radical reducing capability compared to the pyridine-based macrocycle (**L1**).[32] Given the enhanced antioxidant nature of the pyridol-based ligand, we were curious to know whether the antioxidant activity of the pyridol system would be reduced by a change in the position of the hydroxyl group from *p*- to *m*-substituted. We hypothesized that the *m*-hydroxyl ligand would display reduced antioxidant activity, versus the *p*-hydroxyl derivative, arising from the fact that the hydroxyl substituent in **L3** lies in closer proximity to the N-pyridine atom. The *m*-hydroxyl ligand (**L3**) was produced, and the radical reducing capability was measured. Surprisingly, we found that the radical-scavenging capability of the *m*-hydroxyl substituted ligand was equivalent to the *p*-hydroxyl derivative (Figure S1, Supporting Information). We then set out to explore the chemical characteristics of a series of transition metal complexes derived from the N-heterocyclic ligands, in order to determine if the electronic nature of **L2** and **L3** could be differentiated from one another.

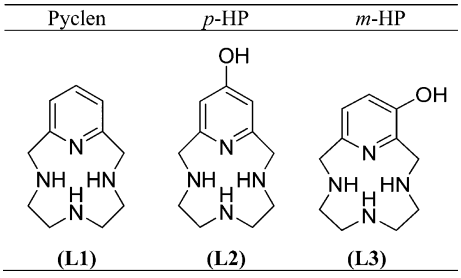

Figure 1. The 12-membered pyridine- and pyridol-containing tetra-aza (N_4) macrocycles investigated in this study.

Herein the syntheses, structural, electronic, and electrochemical properties of **L1**−**L3** and the corresponding metal complexes $[Ni^{II}(\mathbf{L1})(Cl)]_2(ClO_4)_2$ (**1**), $[Ni^{II}(\mathbf{L2})(Cl)]_2(ClO_4)_2$ (**2**), $[Ni^{II}(\mathbf{L3})(Cl)]_2(ClO_4)_2$ (**3**), $[Cu^{II}\mathbf{L1}Cl](ClO_4)$ (**4**), $[Cu^{II}\mathbf{L2}Cl](ClO_4)$ (**5**), $[Cu^{II}\mathbf{L3}Cl](ClO_4)$ (**6**), $[Zn^{II}\mathbf{L1}Cl](ClO_4)$ (**7**), $[Zn^{II}\mathbf{L2}Cl](ClO_4)$ (**8**), and $[Zn^{II}\mathbf{L3}Cl](ClO_4)$ (**9**) are described. This work is significant because it represents a first report on the chemical properties of a series of transition-metal complexes derived from a pyridol-based (12-membered) macrocyclic skeleton. The aim of this work is to understand how the electronic nature of the metal center is altered by a subtle change in the structure of the pyridine ring and in particular to determine if the hydroxyl group acts as an electron-donating or electron-withdrawing substituent, with respect to the metal center. This type of information is useful because it provides fundamental insight into how *m*- and *p*-hydroxylation of the pyridine ring modifies the electronic nature of the π-system and why this subtle change affects the electronic behavior of the metal center.

EXPERIMENTAL SECTION

Caution! Perchlorate salts are explosive and should be handled in small quantities. In particular, such compounds should never be heated as solids. All chemical reagents were purchased from either Sigma Aldrich or Alfa Aesar and used without further purification.

Chemical Preparation of the 12-Membered Pyridine- and Pyridol-Based Tetra-aza Macrocycles L1−L3. The ligands investigated in this study were prepared according to established procedures, which involves the (1 + 1) condensation reaction between the nosylated (Ns) amine segment and the respective benzyl dichloride.[32] Scheme 1 shows the general reaction conditions used for the macrocyclization step and subsequent amine deprotection. The synthetic details regarding **L1** and **L2** have been reported elsewhere, and the full preparative details for the novel ligand *m*-hydroxyl ligand

Scheme 1. General Reactions Conditions Employed for the Marcocyclization Step and Amine Deprotection

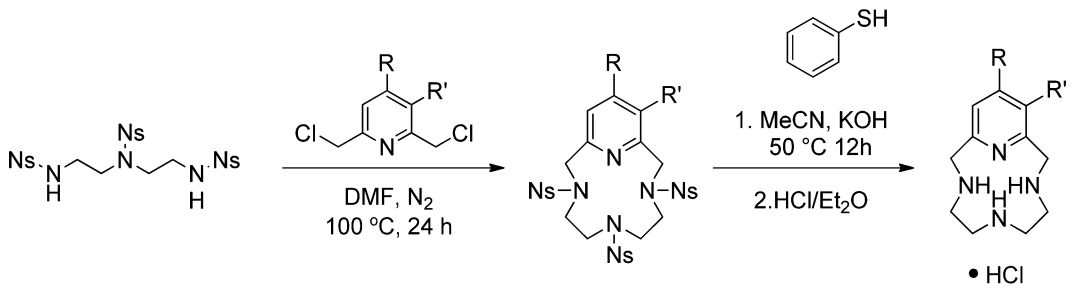

L1: R = H, R' =H, **L2**: R = OBn, R' = H, **L3**: R = H, R' = OBn.

dx.doi.org/10.1021/ic402119s | *Inorg. Chem.* 2014, 53, 1406−1416

Table 1. Crystal Data, Intensity Collections and Structure Refinement Parameters for $[Ni^{II}(L1)(Cl)]_2(ClO_4)_2$ (1), $[Ni^{II}(L2)(Cl)]_2(ClO_4)_2$ (2), $[Cu^{II}(L2)(Cl)](ClO_4)_2$ (5), $[Cu^{II}(L3)(Cl)](ClO_4)$ (6), $[Zn^{II}(L2)(Cl)](ClO_4)$ (8), and $[Zn^{II}(L3)(Cl)](ClO_4)$ (9)

complex	1	2	5	6	8	9
formula	$Ni_2C_{22}H_{36}Cl_4N_8O_8$	$Ni_2C_{22}H_{36}Cl_4N_8O_{10}$	$CuC_{11}H_{18}Cl_2N_4O_5$	$CuC_{11}H_{20}Cl_2N_4O_6$	$ZnC_{11}H_{18}Cl_2N_4O_5$	$Zn_2C_{22}H_{36}Cl4N_8O_{10}\cdot H_2O$
M.W.	799.77	831.77	420.87	438.76	422.57	863.14
unit cell	monoclinic	triclinic	monoclinic	triclinic	monoclinic	monoclinic
space group	$P121/c1$	$P\bar{1}$	$P121/c1$	$P\bar{1}$	$P121/n1$	$P21/c$
a (Å)	7.1569(4)	7.065(4)	11.454(5)	8.0118(10)	11.509(5)	7.783(2)
b (Å)	18.703(10)	10.65(7)	8.985(4)	9.0865(11)	9.0075(4)	26.23(8)
c (Å)	11.304(6)	11.79(7)	18.166(6)	13.227(17)	15.471(7)	17.07(5)
α	90	72.958(16)	90	109.532(3)	90	90
β	97.055(2)	80.072(16)	122.113(19)	93.412(4)	97.410(2)	104.446(13)
γ	90	78.071(17)	90	107.352(3)	90	90
volume (Å^3)	1501.24(14)	825.2(9)	1583.5(11)	852.55(18)	1590.48(12)	3376.0(17)
Z	4	1	4	2	4	4
D_{calc} (g/cm^3)	1.783	1.674	1.777	1.701	1.777	1.698
reflections collected	37488	64453	5146	13671	91677	7744
independent reflections	3797	3671	3545	3617	8871	5483
R_{int}	0.0603	0.0142	0.0255	0.0186	0.0392	0.0458
completeness to θ (%)	99.5	95.9	98.5	95.7	99.3	100
GOF	1.090	1.001	1.024	1.038	1.019	1.054
R_1, wR_2 [$I > 2\sigma(I)$]	0.0363, 0.0889	0.0401, 0.1121	0.0245, 0.0638	0.0407, 0.1179	0.0453, 0.1106	0.0551, 0.1646
R_1, wR_2	0.0426, 0.0918	0.0413, 0.1136	0.0277, 0.0660	0.0453, 0.1221	0.0684, 0.1251	0.0822, 0.1863

(**L3**) can be found in the Supporting Information (Schemes S1−S4). Please note that each of the ligands utilized were isolated as the amine HCl salts, prior to complexation with the metal-ions.

Preparation of the $[(Ni^{II}(N_4)(Cl)]_2(ClO_4)_2$, $[Cu^{II}(N_4)(Cl)](ClO_4)$, and $[Zn^{II}(N_4)(Cl)](ClO_4)$ Complexes (1−9) Derived from the Tetra-aza (N_4) Macrocyclic Ligands of L1−L3. The ligand−metal complexes were all prepared in a similar manner. A 50 mg sample of **L1**, **L2**, or **L3** (HCl salt) was dissolved in 10 mL of deionized water, and the pH of the ligand in solution was adjusted to 10.0 using concentrated potassium hydroxide. Next, a one molar equivalent of the respective $[M^{II}](ClO_4)_2\cdot 6H_2O$ solid salt was added to a stirring solution containing the ligand. The pH of the complex in solution was adjusted to 5.0 with potassium hydroxide, and the complex mixture was stirred overnight at 50 °C. The next day, the solvent was removed under reduced pressure, yielding the crude inorganic complexes as powdery solids. The crude Cu(II) and Zn(II) complexes (**4**−**9**) were taken up in methanol and filtered through a 45 μm syringe to remove the potassium chloride byproduct. The solvent was removed under reduced pressure which yielded the blue Cu(II) and off-white Zn(II) complexes as powdery solids. The crude Ni(II) complexes (**1**−**3**) were first washed with methanol and then filtered through a 45 μm syringe (the observed purple solid is insoluble in methanol). Next, the filter containing the purple precipitate was rinsed with 5 mL of methanol, followed by 10 mL of deionized water in order to elute the desired complex from the filter. The solvent was removed under reduced pressure, which gave complexes **1**−**3** as purple powdery solids.

$[Ni^{II}(L1)(Cl)]_2(ClO_4)_2$ (1). Yield = 58% (33.8 mg, 0.042 mmol). ESI-MS (m/z): found: 263.0017 $[Ni^{II}(\mathbf{L1})\text{-}H]^+$ (100%), theoretical: 263.0885 $[Ni^{II}(\mathbf{L1})\text{-}H]^+$. UV−vis λ_{max}/nm (ε/M$^{-1}\cdot$cm^{-1}): 264 (137), 271 (sh), 563 (14), 779 (sh), and 955 (41). Purple crystals suitable for X-ray structural analysis were obtained by the slow evaporation of water.

$[Ni^{II}(L2)(Cl)]_2(ClO_4)_2$ (2). Yield = 95% (42.9 mg, 0.051 mmol). ESI-MS (m/z): found: 279.1183 $[Ni^{II}(\mathbf{L2})\text{-}H]^+$ (100%), theoretical: 279.0834 $[Ni^{II}(\mathbf{L2})\text{-}H]^+$. UV−vis λ_{max}/nm (ε/M$^{-1}\cdot$cm^{-1}): 246 (200), 556 (16), 784 (sh), and 951 (41). Purple crystals suitable for X-ray structural analysis were obtained in a similar manner as **1**.

$[Ni^{II}(L3)(Cl)]_2(ClO_4)_2$ (3). Yield = 88% (56.0 mg, 0.067 mmol). Extensive attempts were carried out to obtain this complex in a crystalline form suitable for X-ray analysis but failed. ESI-MS (m/z): found: 279.1142 $[Ni^{II}(\mathbf{L3})\text{-}H]^+$ (100%), theoretical: 279.0834 $[Ni^{II}(\mathbf{L2})\text{-}H]^+$. UV−vis λ_{max}/nm (ε/M$^{-1}\cdot$cm^{-1}): 220 (448), 285 (271), 552 (6), 788 (sh), and 947 (12).

$[Cu^{II}(L1)(Cl)](ClO_4)$ (4). Yield = 91% (75.4 mg, 0.186 mmol). The crystal structure for this complex has been reported previously by Busch et al.[33] ESI-MS (m/z): found: 304.0550 $[Cu^{II}(\mathbf{L1})(Cl)]^+$ (100%), theoretical: 304.0516 $[Cu^{II}(\mathbf{L1})(Cl)]^+$. UV−vis λ_{max}/nm (ε/M$^{-1}\cdot$cm^{-1}): 261 (4353), 275−330 (sh), and 713 (109).

$[Cu^{II}(L2)(Cl)](ClO_4)$ (5). Yield 97% (55.5 mg, 0.131 mmol). Aqua blue crystals suitable for X-ray structural analysis were obtained from the slow evaporation of methanol. ESI-MS (m/z): found: 320.0950 $[Cu^{II}(\mathbf{L2})(Cl)]^+$ (100%), theoretical: 320.0465 $[Cu^{II}(\mathbf{L2})(Cl)]^+$. UV−vis λ_{max}/nm (ε/M$^{-1}\cdot$cm^{-1}): 249 (8779), 284−330 (sh), and 699 (107).

$[Cu^{II}(L3)(Cl)](ClO_4)$ (6). Yield 95% (47.6 mg, 0.113 mmol). Teal blue crystals suitable for X-ray analysis were obtained in a manner similar to **5**. ESI-MS (m/z): found: 320.0618 $[Cu^{II}(\mathbf{L3})(Cl)]^+$ (100%), theoretical: 320.0465 $[Cu^{II}(\mathbf{L3})(Cl)]^+$. UV−vis λ_{max}/nm (ε/M$^{-1}\cdot$cm^{-1}): 208 (12454), 246 (7841), 268−350 (sh), and 696 (121).

$[Zn^{II}(L1)(Cl)](ClO_4)$ (7). Yield 91% (85.3 mg, 0.223 mmol). The crystal structure for this complex has been reported previously by Busch et al.[33] ESI-MS (m/z): found: 305.0231 $[Zn^{II}(\mathbf{L1})(Cl)]^+$ (100%), theoretical: 305.0511 $[Zn^{II}(\mathbf{L1})(Cl)]^+$. ^{13}C NMR ($D_2O$) δ: 154.3, 141.2, 121.3, 51.9, 51.8, 50.0, 49.9, and 45.3.

$[Zn^{II}(L2)(Cl)](ClO_4)$ (8). Yield 93% (45.2 mg, 0.106 mmol). Yellow crystals suitable for X-ray analysis were obtained from the slow evaporation of methanol. ESI-MS (m/z): found: 321.0919 $[Zn^{II}(\mathbf{L2})\text{-}(Cl)]^+$ (100%), theoretical: 321.0461 $[Zn^{II}(\mathbf{L2})(Cl)]^+$. ^{13}C NMR ($D_2O$) δ: 168.6, 156.0, 109.2, 51.6, 48.9, 49.0, 45.5, and 45.4.

$[Zn^{II}(L3)(Cl)](ClO_4)$ (9). Yield 91% (50.1 mg, 0.118 mmol). Yellow crystals suitable for X-ray analysis were obtained in a similar manner as **8**. ESI-MS (m/z): found: 321.0942 $[Zn^{II}(\mathbf{L3})(Cl)]^+$ (100%), theoretical: 321.0461 $[Zn^{II}(\mathbf{L3})(Cl)]^+$. ^{13}C NMR ($D_2O$) δ: 149.8, 145.0, 141.8, 126.8, 121.8, 51.3, 50.5, 49.8, 48.9, 48.2, 45.3, and 45.1.

X-ray Crystallography. Crystal diffraction data were collected at 100 K on a Bruker SMART X2S diffractometer, equipped with monochromatic Mo Kα radiation (λ = 0.71073 Å). Data collection, frame integration, data reduction (multiscan), and structure

dx.doi.org/10.1021/ic402119s | Inorg. Chem. 2014, 53, 1406−1416

determination were carried out using APEX2 software. Structural refinements were performed with XShell (v 6.3.1), by the full-matrix least-squares method. All non-hydrogen atoms were refined using anisotropic thermal parameters, while the hydrogen atoms were treated as mixed. The ORTEP molecular plots (50%) were produced using Olex 2. The crystallographic details are combined into Table 1.

Mass Spectrometry. ESI mass spectral analysis were obtained on an Agilent 1200 series 6224 TOF LC/MS spectrometer at 175 V (+ ESI scan) in aqueous solution.

UV−vis Spectrophotometry. The electronic absorption spectra were obtained between 200 and 1100 nm on an 8453 UV−vis spectrophotometer (Agilent) using a 3 mL quartz cuvette with a 1 cm path length. The extinction coefficients of each complex were calculated according to the Beer−Lambert law.

NMR Spectroscopy. ^{1}H and ^{13}C NMR spectra were carried out in deuterated solvents at 25 °C. The spectra of the ligands (**L1**−**L3**) and the respective Zn(II) complexes (**7**−**9**) were measured in D_2O. All spectra were obtained on a Bruker AvanceIII (400 MHz) High Performance Digital NMR spectrometer.

Cyclic Voltammetry. All experiments were performed using a Basi C3 cell stand under a blanket of N_2 associated with a conventional three-electrode electrochemical cell. The system was composed of a carbon working electrode, an $Ag/AgNO_3$ reference electrode, and a Pt counter electrode. All experiments reported were performed at a potential sweep rate of 100 mV·s^{-1}. For electrochemical analysis, 10.0 mg of each complex was dissolved in a 10 mL solution of anhydrous dimethylformamide (DMF) containing tetrabutylammonium tetraflouroborate (10.0 mg) as the supporting electrolyte.

RESULTS AND DISCUSSION

Electronic Properties of the 12-Membered Pyridine- and Pyridol-Based Tetra-aza Macrocyclic Ligands. The electronic properties of **L1**−**L3** were characterized using UV−vis and NMR spectroscopy in aqueous solution. As shown in Figure 2, there is a bathochromic shift in the absorption

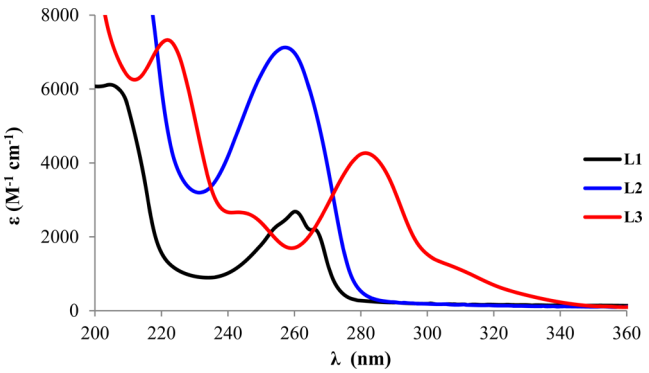

Figure 2. Electronic absorption spectra of the free macrocycles measured in water, at pH 6.0 (25 °C). Extinction coefficients [λ_{max}/nm (ε/M^{-1}·cm^{-1})] for **L1**: 260 (2549), 266 (2203); **L2**: 257 (7125); **L3**: 220 (7233), 248 (sh), and 284 (4168).

maxima following the series **L2** < **L1** < **L3**. This observation agrees with density functional theory (DFT) theoretical calculations (Figure S2, Supporting Information) that show the difference in energy between the HOMO−LUMO molecular orbitals of the ligands follows a similar trend: **L3** (ΔE = 249 kJ/mol) > **L2** (ΔE = 421 kJ/mol) ≥ **L1** (ΔE = 491 kJ/mol). Hydroxylation of the pyridine ring gives rise to significantly more intense $\pi \rightarrow \pi^*$ charge transfer bands, suggesting that the π-bonding interactions are stronger in pyridol systems of **L2** [257 nm (7125)] and **L3** [20 nm (7233) and 284 nm (4168)], versus the pyridine system [(**L1**) 260 nm (2549) and 266 nm (2203)]. Additionally, the spectrum of the *m*-substituted ligand displays a greater amount of charge transfer character versus either **L1** or **L2** and indicates that the electronic nature of the aromatic system of **L3** has an increased level of perturbation. This behavior is attributed to the asymmetric nature of the *m*-hydroxyl substituted backbone.

The ^{13}C NMR spectra for **L1**−**L3** are represented in Figure 3a. The most significant feature to be noted is that the signals pertaining to **L1** (124.1 ppm to 149.9 ppm) and **L3** (125.3 ppm to 151.5 ppm) lie within close proximity to each other, while those of **L2** (111.5 ppm to 166.2 ppm) show a greater separation. This feature suggests that the hydroxyl substituent exerts an electron-donating (resonance) effect that is dependent upon the substitution pattern, with respect to the N-pyridine atom. To understand the chemical nature behind these shifts, the resonance structures which represent the delocalization of an oxygen atom lone pair into the aromatic system of **L2** and **L3** must be considered (Figure 3b). For the *p*-substituted ligand (blue), a lone pair on the oxygen atom can be delocalized onto C(2), C(4), and the pyridine nitrogen atom, but for the *m*-substituted ligand (red) the electronic charge density can only delocalize onto atoms C(1), C(3), and C(5). This difference is significant because the lone pair never resides directly on the nitrogen atom in **L3**, and as a result the negative charge is stabilized by a lesser extent, when compared to **L2**. A correspondent upfield shift is observed for **L2** at 111.5 ppm, arising from the delocalization of the lone pair onto C(2) and C(4). Concomitantly, in the spectrum of **L2**, there is a considerable downfield shift at 166.2 ppm assigned to C(1) and C(5) as the lone pair cannot delocalize onto these atoms.

Structural Properties of the Six-Coordinate Complexes $[Ni^{II}(L1)(Cl)]_2(ClO_4)_2$ (1) and $[Ni^{II}(L2)(Cl)]_2(ClO_4)_2$ (2). Solid-state structures containing the first-row 3d transition metals Mn(III), Fe(III), Cu(II), and Zn(II) coordinated to **L1** have been reported previously.[33] The structure for the Ni(II) complex is yet to be reported; therefore, crystals suitable for X-ray diffraction analysis were obtained for comparison to the pyridol-based systems. Repeated attempts to isolate complex **3** as a crystalline solid suitable for X-ray analysis were unsuccessful and further complicated by the fact that **1**−**3** are strictly water-soluble. This anomaly is potentially a result of the chiral nature of the metal complex formed, where the solid-state structure of **3** would lack a mirror plane and an inversion center. The molecular structures of the Ni(II) complexes **1** and **2** are depicted in Figure 4, with the selected bond lengths and angles listed in Table 2. The structures of complexes **1** and **2** are observed to be dimeric species in the solid-state. The Ni(II) ion is ligated by the N atoms N(1), N(2), N(3), and N(4) of the ligand backbones and bridged by two Cl atoms [Cl(1) and Cl(1′)], giving rise to a symmetrically identical complex. The macrocyclic ligands **L1** and **L2** present cis-folded (N_4) configurations, giving precedence to the idea that the 12-membered cavity is not spacious enough to allow the coplanar coordination of the Ni(II) ion by the ligand.[18,23,29,34] All of the Ni−N bond lengths for the pyridine-based (**1**) complex (2.133−1.997 Å) are shorter than those for the corresponding pyridol-based (**2**) complex (2.146−2.013 Å). This contraction indicates that the bonding interaction between the Ni(II) and nitrogen atoms weakens slightly. Likewise, the distances between the neighboring Ni(II) and Cl atoms are increased for complex **2** and is consistent with a decrease in Lewis-acidity of the metal center as result of *p*-hydroxyl functionalization.

Electronic Properties of the Six-Coordinate Complexes $[Ni^{II}(L1)(Cl)]_2(ClO_4)_2$ (1), $[Ni^{II}(L2)(Cl)]_2(ClO_4)_2$ (2),

dx.doi.org/10.1021/ic402119s | Inorg. Chem. 2014, 53, 1406−1416

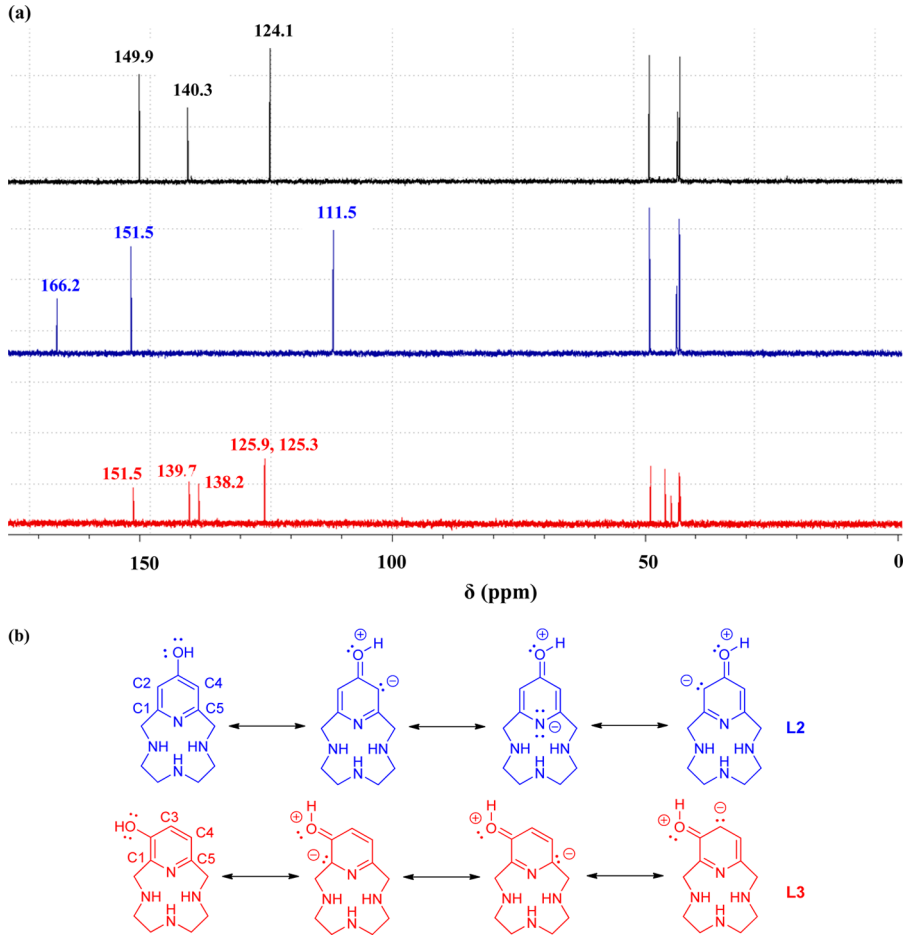

Figure 3. (a) Overlay of the ^{13}C NMR spectra of **L1**−**L3**, measured in D_2O solution, (pH = 6.0). **L1**: δ = 149.9, 140.3, 124.1, 49.1, 43.5, 43.0; **L2**: δ = 166.2, 151.5, 111.5, 49.0, 43.7, 43.1; **L3**: δ = 151.5, 139.7, 138.2, 125.9, 125.3, 48.6, 45.6, 44.4, 43.4, 43.1, 42.5. (b) Shown are the structures of the intermediate compounds which contribute to the resonance hybrid of **L2** (red) and **L3** (blue), resulting from the delocalization of an oxygen atom lone pair into the aromatic system.

and $[Ni^{II}(L3)(Cl)]_2(ClO_4)_2$ (3). The absorption spectra of the violet Ni(II) complexes were obtained in aqueous solution, and are shown in Figure 5. No color changed was observed when the complexes were dissolved in water. A blue-shift in the absorbance maxima is observed across the series from **3** [285 nm (271)], to **1** [264 nm (137)], to **2** [246 nm (200)], which is consistent with the spectrum obtained for **L1**−**L3**. Again, the pyridol-based complexes (**2** and **3**) have larger extinction coefficients ($\pi \rightarrow \pi^*$) than the pyridine-based complex (**1**), suggesting the π-bonding interactions are strengthened in response to hydroxylation. Additionally, complex **3** contains an intense high energy band at 220 nm (448) also noted to be unique in the spectra of **L3** (Figure 5). Furthermore, two lower energy transitions ranging from 450 to 1100 nm are observed in the spectra of the Ni(II) derivatives. The pyridine-based (**1**) [563 (14) and 955 (41)] and *p*-hydroxyl (**2**) [556 (16) and 951 (41)] complexes have larger extinction coefficients than the *m*-hydroxyl derivative (**3**) [552 (6) and 947 (12)].

It should be noted, however, that Ni(II) complexes derived from tetra-aza ligands containing a ring size greater than 12-membered exist in solution as an equilibrium mixture of six-coordinate (blue), and four-coordinate (yellow) species.[19−21,23,29,35−40] The electronic spectra of the four-coordinate Ni(II) species are characterized by the presence of absorption bands that are confined between 300 to 600 nm and normally contain λ_{max} values not to exceed 500 nm.[20,21,27,29,30,37−41] The complexes described here lack the presence of absorption bands in the range between 320 to 490 nm and are inconsistent with the electronic spectra defined by a four-coordinate Ni(II) species. Furthermore, Busch and co-workers have established that most six-coordinate Ni(II) tetra-aza complexes are paramagnetic, green or violet, with characteristically low extinction coefficients.[35,36] These attributes are consistent with the complex systems reported here, and to date not a single report exists that provides evidence for the existence of a four-coordinate Ni(II) complex derived from a 12-memebred tetra-aza ligand.[29] It is currently postulated that the six-coordinate Ni(II) species that were isolated in the solid-state exist in solution as well. However, it is plausible that an exchange reaction between the chlorine ligand and solvent molecule could occur, resulting from the dissociation of the dimeric Ni(II) species in solution.

Electrochemical Properties of the Six-Coordinate Complexes $[Ni^{II}(L1)(Cl)]_2(ClO_4)_2$ (1), $[Ni^{II}(L2)(Cl)]_2(ClO_4)_2$ (2), and $[Ni^{II}(L3)(Cl)]_2(ClO_4)_2$ (3). Electrochemical experiments carried out on complexes **1**−**3** in DMF and aqueous solvents yielded ill-defined and irreproducible cyclic voltammetry (CVs) results, respectively. The former result is likely due to poor solubility of the Ni(II) complexes in DMF. Fabbrizzi et al. reported similar inconsistent electrochemical behavior for an octahedral, 12-membered dioxo tetra-aza macro-cyclic Ni(II) complex.[2] Ghachtonli and co-workers also

dx.doi.org/10.1021/ic402119s | Inorg. Chem. 2014, 53, 1406−1416

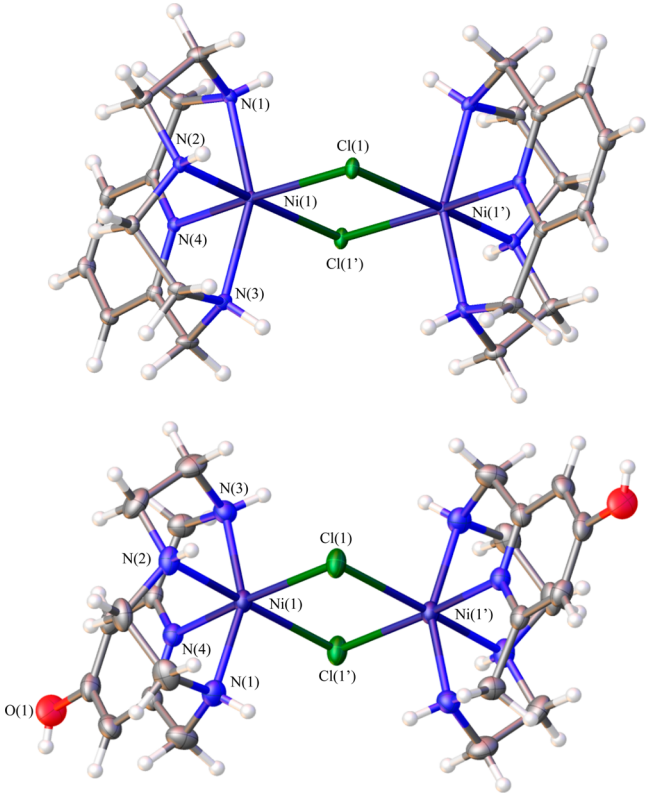

Figure 4. ORTEP drawing of the six-coordinate Ni(II) complexes **1** (top) and **2** (bottom) showing the presence of a Ni(μ-Cl)$_2$Ni bridge, with the labeling scheme adopted. The two perchlorate counterions have been omitted for clarity.

Table 2. Selected Bond Lengths (Å) and Bond Angles (°) for the Six-Coordinate Complexes: $[Ni^{II}(L1)(Cl)]_2(ClO_4)_2$ (1) and $[Ni^{II}(L2)(Cl)]_2(ClO_4)_2$ (2)

complex	1	2
Ni–N(1)	2.133(2)	2.142(3)
Ni–N(2)	2.077(2)	2.087(2)
Ni–N(3)	2.125(2)	2.146(3)
Ni–N(4)	1.997(1)	2.013(2)
Ni–Cl(1)	2.383(1)	2.416(3)
Ni–Cl(1′)	2.462(7)	2.482(14)
Ni(1)–Ni(1′)	3.572	3.613
Cl(1)–Cl(1′)	3.274	3.307
N(1)–Ni–N(3)	155.4(9)	155.0(9)
N(2)–Ni–Cl(1)	176.0(6)	175.0(6)
N(4)–Ni–Cl(1)	172.9(6)	174.0(6)

reported correspondent behavior for a six-coordinate Ni(II) species derived from the cyclen backbone (12-membered).[10] Conversely, Ni(II) complexes derived from larger 14-, 15-, and 16-membered tetra-aza (unsaturated) ligands are capable of accommodating Ni(I) and Ni(III) valence states rather efficiently, arising from the fact that the four-coordinate complex species prevail in solution.[16,20,21,23,29,30,42] Taken together, these results suggests that the high coordination number imposed by the 12-membered ring system prevents the effective accommodation of Ni(I) and Ni(III) species in solution.

Structural Properties of the Five-Coordinate [Cu(II)-Cl](ClO$_4$) and [Zn(II)Cl](ClO$_4$) Complexes (4–9). In analogy with the solid-state structures for complexes **4** and **7**, the pyridol-based complexes **5**, **6**, **8**, and **9** are five-coordinate and deviate between square-pyramidal and trigonal-bipyramidal geometries.[33] Calculation of the angular geometric parameter (τ) was utilized in order to quantitate the percentage by which the $[Cu^{II}(\mathbf{N_4})Cl]^+$ and $[Zn^{II}(\mathbf{N_4})Cl]^+$ complexes are distorted away from square-pyramidal.[43−45] The τ-value was calculated according to the formula defined by Addison [$\tau = (\beta - \alpha)/60$], where α° = N(4)–M–Cl(1) and β° = N(1)–M–N(3) are the angles that define the basal plane.[45] Please note that for a perfect square-pyramidal species τ = 0.00, and for a perfect trigonal-bipyramidal species, τ = 1.00. The molecular structures of the pyridol-based Cu(II) and Zn(II) complexes are depicted in Figure 6, and the selected metric parameters of **4**–**9** are listed in Table 3. The basal plane is defined by the position of the donor atoms N(1), N(3), N(4), Cl(1), with N(2) as the axial donor.

As shown in Figure 6, the pyridol-derived complexes each present cis-folded geometric arrangements where the metal-ion lies outside the N$_4$ plane.[46,47] The bond lengths for complexes **4**–**9** follow the expected periodic trends, increasing from Cu(II) to Zn(II), with an exception occurring for the axial Zn–N(2) bond lengths (Table 3). The axial Cu–N(2) and Zn–N(2) bond lengths increase by 0.132 Å in **5**, 0.096 Å in **6**, 0.039 Å in **8**, and 0.029 Å in **9** upon hydroxylation of the pyridine ring. This result indicates that the axial M–N(2) bonding interaction is destabilized in response to hydroxylation; this effect is more pronounced for the complexes derived from **L2**. Another significant trend to be noted is that the basal M–Cl(1) and M–N(4) bond distances are shorter for the pyridol-derived complex systems. This contraction indicates that the π-bonding interactions are stronger for the pyridol-based complexes (**5**, **6**, **8**, and **9**) versus the pyridine-based complexes (**4** and **7**). The Cu–Cl(1) bond lengths decrease, significantly, by 0.140 Å in **5**, and 0.101 Å in **6**, while the Zn–Cl(1) bond lengths decrease only slightly.

Crystal field theory predicts that the dz^2 orbital is significantly destabilized when the metal-ion is coordinated in a trigonal-bipyramidal environment, arising from the fact that the axial bonding interactions are stronger in the *z*-axis than in the *xy*-plane. Conversely, a destabilized dx^2-y^2 orbital results from the strengthened in-plane *xy*-bonding interactions in a square-pyramidal environment. The degree by which the five-coordinate complexes deviate away from square-pyramidal is modulated by the strength of the in-plane M–N(4) and M–Cl(1) bonds. As seen experimentally, complexes **5** (τ = 0.07), **6** (τ = 0.20), and **8** (τ = 0.16) are distorted closer toward square pyramidal while **4** (τ = 0.63), **7** (τ = 0.42) and **9** (τ = 0.43) deviate further away. This observation leads to the conclusion that complexes that contain stronger basal M–N(4) and M–C(1) bonds and weaker N–N(2) interactions present distortions that lie closer toward square-pyramidal.[28] For each of these cases, the Cu(II) and Zn(II) complexes derived from **L2** are least distorted from square pyramidal and suggests that *p*-hydroxylation imposes a stronger basal ligand-field about the metal center compared to *m*-hydroxylation.

Lastly, the metric parameters related to the aromatic system for the pyridol-based complexes reveal some noteworthy points. The most striking feature to be noted is that the C–O(1) bond lengths for the *p*-hydroxyl complexes (**5** and **8**) are shorter by 0.101 Å and 0.014 Å, respectively, than those for the complexes derived from the *m*-hydroxyl ligand (**6** and **9**). A shorter C–O bond length is consistent with the idea that the C–O bond of **L2** has more partial double-bond character than

dx.doi.org/10.1021/ic402119s | Inorg. Chem. 2014, 53, 1406−1416

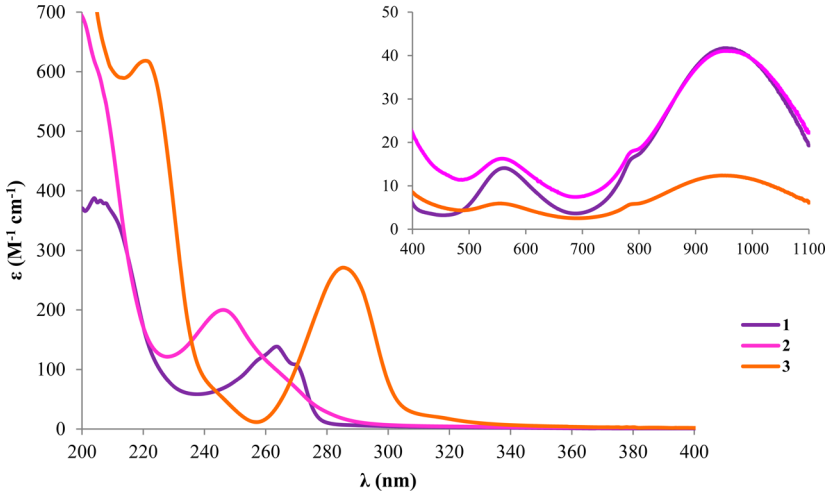

Figure 5. The electronic absorption spectra for $[Ni^{II}(\mathbf{L1})(Cl)]_2(ClO_4)_2$ (**1**), $[Ni^{II}(\mathbf{L2})(Cl)]_2(ClO_4)_2$ (**2**), and $[Ni^{II}(\mathbf{L3})(Cl)]_2(ClO_4)_2$ (**3**) measured in water, at pH 6.0 (25 °C). The inset shows the spectra in the range between 400 and 1000 nm. Extinction coefficients [λ_{max}/nm (ε/M^{-1}·cm^{-1})] for (**1**): 264 (137), 271 (sh), 563 (14), 779 (sh), and 955 (41); (**2**): 246 (200), 556 (16), 784 (sh), and 951 (41); (**3**): 220 (448), 285 (268), 552 (6), 788 (sh), and 947 (12).

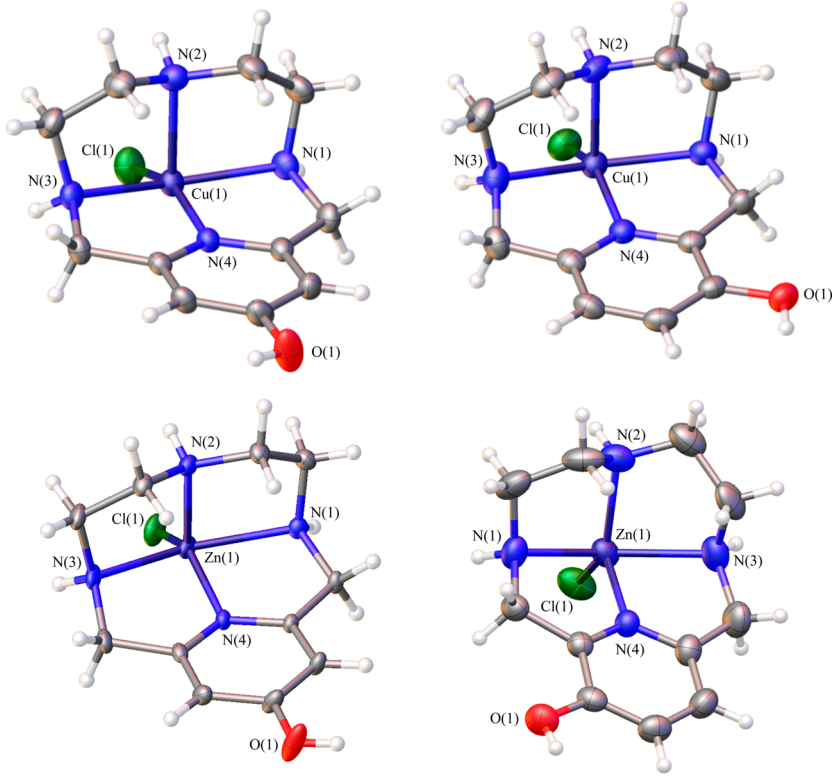

Figure 6. ORTEP representations of the five-coordinate pyridol-based Cu(II) and Zn(II) complexes, **5** (top left) exhibiting a 7%, **6** (top right) a 20% distortion, **8** (bottom left) a 16%, and **9** (bottom right) a 43% distortion from square-pyramidal, with labeling scheme adopted. The perchlorate counterions and solvent molecules (H_2O in **9**) comprising the asymmetric units have been omitted for clarity.

that of **L3** and indicates that the lone pair of the oxygen atom is delocalized to a greater extent throughout the aromatic system of **L2**. Correspondingly, the O(1)−H(1) bond distances are shorter in the *p*-substituted complexes, compared to the *m*-hydroxyl derivatives. These observations suggest that the pyridol ring of complex **5** contains the greatest amount of electronic charge density and is supported by the upfield shift noted in the ^{13}C NMR spectra of **L2** (Figure 3a) and in the corresponding Zn(II) complex spectra discussed in greater detail below.

Electronic and Electrochemical Properties of the Five-Coordinate [Cu(II)Cl](ClO$_4$) and [Zn(II)Cl](ClO$_4$) Complexes (4−9). The electronic spectra of the Cu(II) complexes were measured in water and are shown in Figure 7. Again, no color change was observed when the complexes were dissolved in aqueous solution. In the UV region of the spectra, complexes **4** [261 (4353)], **5** [249 (8779)], and **6** [208 (12454), 246 (7841)] contain broader and more intense $\pi \rightarrow \pi^*$ transitions compared to the spectra of **L1**−**L3**. This result signifies that the π-bonding interactions become stronger in response to Cu(II)

dx.doi.org/10.1021/ic402119s | *Inorg. Chem.* 2014, 53, 1406−1416

Table 3. Selected Bond Lengths (Å) and Bond Angles (°) for the Five-Coordinate Complexes $[Cu^{II}(L1)(Cl)](ClO_4)$ (4), $[Cu^{II}(L2)(Cl)](ClO_4)$ (5), $[Cu^{II}(L3)(Cl)](ClO_4)$ (6), $[Zn^{II}(L1)(Cl)](ClO_4)$ (7), $[Zn^{II}(L2)(Cl)](ClO_4)$ (8), and $[Zn^{II}(L3)(Cl)](ClO_4)$ (9)[a]

complex	4	5	6	7	8	9
M−N(1)	2.052(4)	2.082(16)	2.060(2)	2.245(2)	2.207(17)	2.214(5)
M−N(2)	2.041(3)	2.173(19)	2.137(2)	2.048(1)	2.087(19)	2.060(5)
M−N(3)	2.045(4)	2.079(16)	2.063(2)	2.212(2)	2.209(19)	2.226(5)
M−N(4)	1.963(3)	1.939(16)	1.952(2)	2.055(2)	2.041(17)	2.059(4)
M−Cl(1)	2.365(1)	2.226(9)	2.264(7)	2.245(6)	2.214(6)	2.234(5)
C−O(1)		1.340(4)	1.361(1)		1.339(3)	1.353(3)
O(1)−H		0.819(2)	0.920(1)		0.840(2)	0.850(2)
N(1)−M−N(3)	153.3(1)	158.5(6)	159.6(9)	145.1(6)	153.3(7)	145.5(15)
N(4)−M−Cl(1)	115.8(1)	154.2(7)	147.6(6)	119.8(5)	143.5(5)	119.8(12)
τ-value	*0.63*	*0.07*	*0.20*	*0.42*	*0.16*	*0.43*

[a]The structural parameters for **4** (CCDC # 639155) and **7** (CCDC # 628572) were obtained from the Cambridge Crystallographic Data Center.[33]

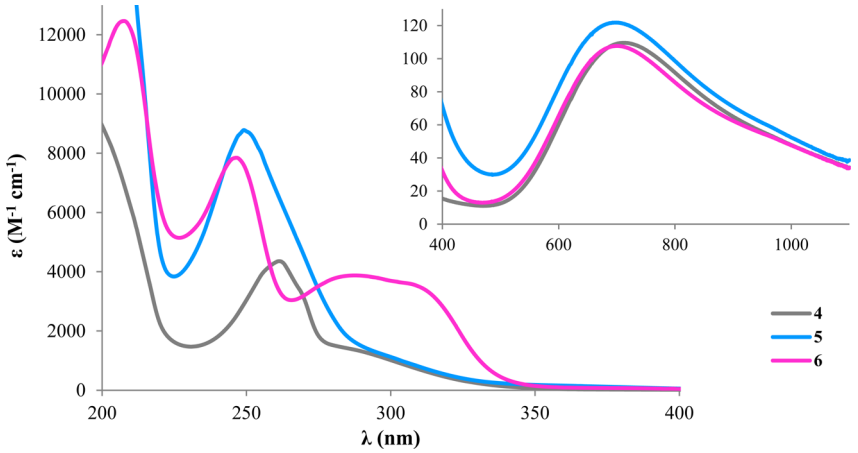

Figure 7. Electronic absorption spectra of $[Cu^{II}(\mathbf{L1})(Cl)]^+$ (**4**), $[Cu^{II}(\mathbf{L2})(Cl)]^+$ (**5**), and $[Cu^{II}(\mathbf{L3})(Cl)]^+$ (**6**) measured in water, at pH 6.0 (25 °C). The inset shows the spectra in the range between 500 and 1000 nm. Extinction coefficients [λ_{max}/nm (ε/M^{-1}·cm^{-1})] for (**4**): 261 (4353), 275−330 (sh), and 713 (109); (**5**): 249 (8779), 284−330 (sh), and 699 (107); (**6**): 208 (12454), 246 (7841), 268−350 (sh), and 696 (121).

coordination.[43] The absorbance maximum of **5** is blue-shifted by 8 nm, versus the maxima for **L2**. The weak shoulder peak that appears around 248 nm for the *m*-substituted ligand becomes a well-defined electronic transition in complex **6**, indicating that metal complexation significantly perturbs the energy of this transition. Furthermore, the extinction coefficients pertaining to complexes **5** and **6** in the UV region of the spectrum are much larger than in complex **4**. This result implies that there is a greater amount of π-density residing throughout the pyridol systems versus the pyridine system, and this effect is more pronounced for **L2** than **L3**. In the visible portion of the spectrum, the blue-colored Cu(II) complexes each contain a single broad absorption band assigned as Cu-based d−d electronic transitions. The absorption maxima for the pyridol complexes blue-shift by 14 nm (**5**) and 17 nm (**6**), with respect to the maximum for **4** (λ_{max} = 713 nm). This feature is consistent with the fact that **5** (τ = 0.07) and **6** (τ = 0.20) present similar geometries in the solid-state, compared to **4** (τ = 0.63), and suggests that the electronic behavior of the Cu(II) ion is affected by the presence of the hydroxyl group. These findings suggest that the lone pair from the oxygen atom is delocalized throughout the aromatic system, and hydroxyl functionalization of the pyridine ring effectively allows for an extension of π-conjugation and is consistent with the conclusions drawn above from the solid-state studies.

CV was used to the characterize the redox behavior of the Cu(II) and Zn(II) complex systems, in order to determine if the electronic nature of the metal center is affected by the structural modifications made to **L1**. The electrochemical activity of each complex was studied in both aqueous solution and dimethylformamide (DMF). We found that the use of DMF as a solvent gave rise to more reproducible CV scans, versus the studies performed in aqueous solution (despite the partial solubility of **5** and **6** in DMF). All of the complexes reported here undergo quasi-reversible Cu(III)/Cu(II) and Cu(II)/Cu(I) redox cycles, separated by a potential of ∼1.00 V, when scanned in the cathodic direction, which are coupled to ligand-based oxidations and reductions, respectively.[16,21,28] The more anodic charge transfer process is always coupled to a ligand-based oxidation (E_{pa} ≈ 800 mV) and is assigned as the Cu(III)/Cu(II) redox cycle.[2,16,21,22,25,28,48,49] Conversely, the more cathodic charge transfer process is assigned as the Cu(II)/Cu(I) redox cycle.[16,21,26,28] The ligand-based redox assignments were made based on the CVs of the Zn(II) complexes (**7**−**9**). As expected, no Zn-based redox activity is observed for complexes **7**−**9** in DMF solution; however, similar ligand-based events noted for both the Cu(II) complexes are present (shown in Figure S3, Supporting Information). Figure 8a,b shows the CVs obtained when complexes **4**−**6** were scanned continuously between 1.10 V and −1.60 V starting

dx.doi.org/10.1021/ic402119s | Inorg. Chem. 2014, 53, 1406−1416

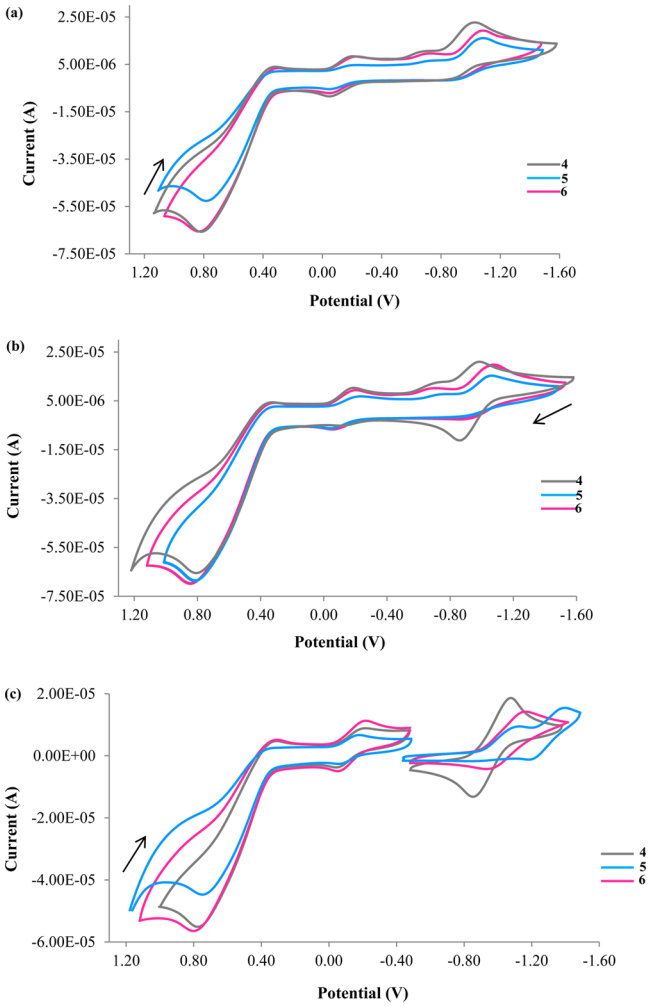

Figure 8. Cyclic voltammograms obtained for the Cu(II) complexes (**4**–**6**) in 10 mL of DMF containing tetrabutylammonium tetrafluoroborate (10 mg) as the supporting electrolyte at a scan rate of 100 mV/s. The first two figures show the CVs obtained for each complex scanned from the (a) cathodic-to-anodic and (b) anodic-to-cathodic direction (from 1.10 V to −1.60 V), and (c) between 1.10 and 0.50 V, and 0.40 and 1.60 V. The potential values presented here have been normalized to the half-wave potential of the Fc(III)/Fc(II) redox couple ($E_{1/2}$ = 0.00 V).

from the anodic and cathodic directions, respectively. The Cu-based redox processes were also studied individually, as well, and the resulting CVs are shown in Figure 8c. The $E_{1/2}$ values for each redox cycle were calculated according to the data presented in Figure 8c and are listed in Table 4. These results are discussed in greater detail below.

The Cu(III)/Cu(II) Redox Couple. An attempt to separate the Cu(III)/Cu(II) redox processes from the more anodic ligand-based oxidation resulted in the absence of a current response. In each case examined when the window of the scan was confined between 200 mV to −500 mV, the current of the system remained essentially constant and the resulting CVs lacked definition (data not shown). As shown in Figure 8c, the Cu(III)/Cu(II) redox couple was only observed when a potential greater than 800 mV was applied to each complex. This result suggests that the ligands must first undergo oxidation in order to accommodate the higher valent Cu(III) species. The easiest attainment of the Cu(III) state, which is defined by the more negative value of the half-wave potential,

Table 4. $E_{1/2}$ Values (V) for 4–6 for the Cu(III)/Cu(II) and Cu(II)/Cu(I) Redox Processes[a]

complex	Cu(III)/Cu(II)	Cu(II)/Cu(I)	ligand [E_{pa} (mV)]
4	−0.12	−0.96	761
5	−0.083	−1.20	735
6	−0.14	−1.05	790

[a]The potential measurements were conducted using a glassy carbon working electrode, a platinum auxiliary electrode, and $Ag^+/AgNO_3$ reference electrode, at a scan rate of 100 mV/s. The data reported here has been normalized to the value of the half-wave potential for the Fc(III)/Fc(II) redox couple.

occurs with the *p*-hydroxyl substituted ligand (Table 4 and Figure 8c). A modification in the position or removal of the hydroxyl substituent results in a more positive $E_{1/2}$ value and is a reflection of how the position of the hydroxyl moiety influences the Lewis-acidity of the copper center. This result implies that the Cu center of **5** ($E_{1/2}$ = −0.083 V) is more electron-rich than that of either **4** ($E_{1/2}$ = −0.12 V) or **6** ($E_{1/2}$ = −0.14 V), suggesting that the electron-donating capacity of the macrocycle increases in the order **L2** > **L1** ≥ **L3**. This trend correlates with the blue-shift observed in the electronic spectra of **4**–**6** and is postulated to be a consequence of the enhanced π-bonding interactions of **L2** between the aromatic system, chlorine atom, and metal center. The stronger *xy*-plane interactions displayed by **5** observed both in the solid-state and in solution correlate with the strength of the Cu−N(4) and Cu−(Cl) π-bonding interactions. The **L2** derivative imposes a stronger basal interaction with the Cu(II) center compared to **L1** and **L3** and allows for an easier attainment of the Cu(III) oxidation state.[2,15,20,21,28,29,34]

The Cu(II)/Cu(I) Redox Couple. As complex **4** is scanned from the cathodic to the anodic direction the Cu(II)/Cu(I) redox cycle becomes a more favorable process. As seen in Figure 8b, the peak corresponding to the oxidation of Cu(I) [E_{pa} = −850 mV] is well-defined for the pyridine-based complex **4** versus the pyridol-derived complexes, where the peaks for complexes **5** and **6** are similar in shape and intensity to those in Figure 8a. Moreover, consecutive cycles (two or greater) gave rise to a significant reduction in the peak intensity of **4** similar to the CV shown in Figure 8a. It should be noted that the repeated cycles result in no loss of current intensity for the remaining peaks. When the scan window of each complex is restricted to a more cathodic potential (−0.40 V to −1.60 V) the oxidation of Cu(I) becomes a more favorable process for **4** and **6**, than for **5**. This idea is evidenced by the significant increase in the current intensity for **4** and **6** observed in Figure 8c, versus the current values in Figure 8a.

In either case, the oxidation of Cu(I) is least favorable for complex **5** and is independent of the scan window. This result implies that the *p*-hydroxyl ligand is not well-suited to accommodate the Cu(II)/Cu(I) redox cycle in the DMF solution. Furthermore, the ligand-based oxidation that is coupled to the Cu(II)/Cu(I) redox process is no longer observed for complexes **4** and **6** but remains present in complex **5**. This behavior suggests that when a more cathodic potential is applied to the system, the oxidation of Cu(I) becomes a more favorable or reversible process concomitant to the absence of the ligand-based reduction. Lastly, the easiest attainment of the Cu(I) oxidation state, which is defined by the least negative half-wave potential, occurs with the pyridine-based ligand (Table 4). The same trend noted for the Cu(III)/

dx.doi.org/10.1021/ic402119s | Inorg. Chem. 2014, 53, 1406−1416

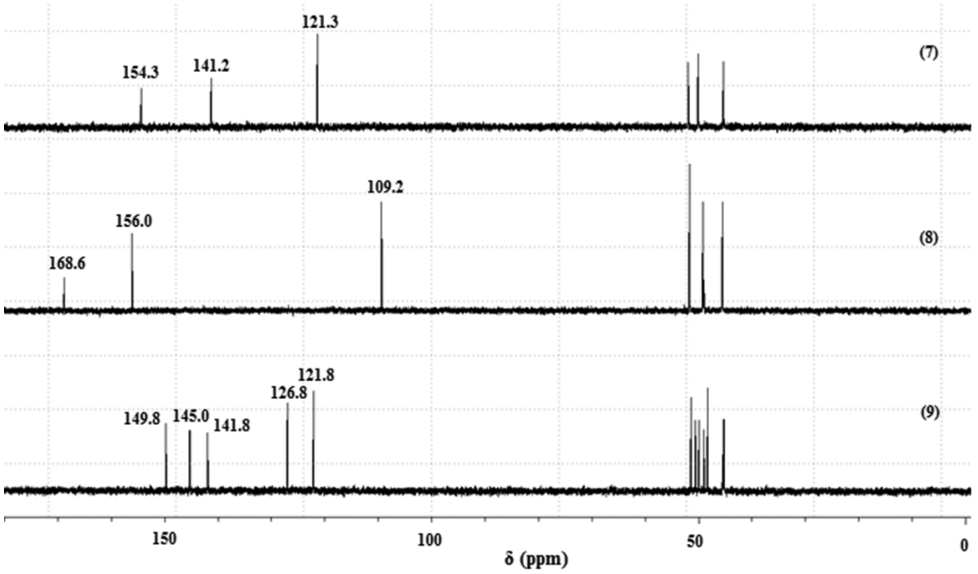

Figure 9. Overlay of the ^{13}C NMR spectra of the Zn(II) complexes (**7**–**9**) measured in D_2O solution (pH = 6.0). **7**: δ = 154.3, 141.2, 121.3, 51.9, 51.8, 50.0, 49.9, 45.3; **8**: δ = 168.6, 156.0, 109.2, 51.6, 49.0, 48.9, 45.5, 45.4; **9**: δ = 149.8, 145.0, 141.8, 126.8, 121.8, 51.3, 50.5, 49.8, 48.2, 45.3, 45.1.

Cu(II) processes is observed for the Cu(II)/Cu(I) cycle. This result implies that the Cu center of **5** ($E_{1/2}$ = −1.20 V) is more electron-rich than that of either **4** ($E_{1/2}$ = −0.96 V) or **6** ($E_{1/2}$ = −1.05 V) and suggests that the electron-donating capacity of the ligands increases across the series **L2** > **L1** > **L3**, which correlates with the blue-shift observed in the electronic spectra of **4**–**6**.

The electronic properties of the Zn(II) complexes were characterized via NMR spectroscopy in D_2O solution, and the resulting spectra are presented in Figure 9. The information inferred from the spectra is consistent with the involvement of the three aliphatic and single pyridine nitrogen atoms in a nonplanar fashion, with respect to the metal cation. Notably, the ^{13}C NMR spectra of **7** and **8** show eight resonances, which contain two additional peaks compared to the spectra for **L1** and **L2**. The benzyl carbon atoms retain chemical equivalence, but the four aliphatic carbon atoms composing the lower and more flexible portion of the ligand lose chemical equivalence upon coordination of Zn(II). The result is suggestive of a nonplanar and less symmetric carbon framework in solution versus the free macrocycles. These findings are consistent with the results obtained in the solid-state studies, as the ligands display a cis-folded conformation where the metal-ion lies outside the N_4 plane. In addition, the trends noted for the resonance signals related to the aromatic carbon atoms of **L1**–**L3** are conserved in the ^{13}C NMR spectra of complexes **7**–**9** as well. As noted previously, the upfield shift in the resonance signal observed for complex **8** (109.2 ppm) is supportive of the conclusion that the *p*-pyridol system is more electron donating that the *m*-substituted pyridol system and is reflected by the electrochemical behavior of the Cu(II) complexes discussed above.

CONCLUSION

Effect of *p*- versus *m*-Hydroxylation. The data presented throughout this study support the idea that introduction of the hydroxyl substituent leads to an increase in the amount of electronic charge density throughout the pyridine ring. Clearly, *p*-hydroxylation induces a larger electron-donating effect than *m*-hydroxylation with respect to the metal center. Overall, the results of this study reveal that the Lewis-basicity of the 12-membered pyridine- and pyridol-based tetra-aza macrocyclic ligands increases across the series **L2** > **L1** > **L3**. The asymmetric nature of the *m*-hydroxyl ligand masks any of the electron-donating ability gained upon hydroxylation of the pyridine ring. Future work will focus on isolation and characterization of the Cu(III) species derived from **4**–**6**, via chemical oxidation and controlled potential electrolysis.[2,28,49–51] Notably, the formation of intermediate Cu(III) species is thought to be an essential component for the assembly of C–C and C-heteroatom bonds for Cu/ligand-catalyzed cross-coupling reactions.[17,52] The ligand sets presented herein display the ability to accommodate both Cu(I) and Cu(III) oxidation states in solution and should be considered toward catalysis of this type.

ASSOCIATED CONTENT

Supporting Information

Crystallographic data for **1**, **2**, **5**, **6**, **8**, and **9** (CCDC #: 950044, 950046, 950045, 911993, 950047 and 947495, respectively) in both CIF and table format. This material is available free of charge via the Internet at http://pubs.acs.org.

AUTHOR INFORMATION

Corresponding Author

*E-mail: kayla.green@tcu.edu.

Notes

The authors declare no competing financial interest.

ACKNOWLEDGMENTS

The authors are grateful for generous financial support from the TCU Andrews Institute of Mathematics & Science Education, TCU Research and Creativity Grants (to K.G.), TCU SERC (to M.E.O. and T.H.), and the Robert A. Welch Foundation (to K.G., P-1760). We sincerely thank the group of Dr. Eric Simanek for access to mass spectrometry and Dr. Tracy Hanna for helpful conversations related to this project. In addition, we are grateful to Zoltan Kovacs (UTSW) for the sole contribution of **L1** and Charles Campana for XRD advice.

REFERENCES

(1) Curtis, N. F. *J. Chem. Soc., Dalton Trans.* **1974**, 347−350.
(2) Fabbrizzi, L.; Kaden, T. A.; Perotti, A.; Seghi, B.; Siegfried, L. *Inorg. Chem.* **1986**, *25*, 321−327.
(3) Esteves, C. V.; Lima, P. M.; Delgado, R.; Brandao, P.; Felix, V. *Dalton Trans.* **2013**, *42*, 6149−6160.
(4) Bernier, N.; Costa, J.; Delgado, R.; Felix, V.; Royal, G.; Tripier, R. *Dalton Trans.* **2011**, *40*, 4514−4526.
(5) Green, K. N.; Viswanathan, S.; Rojas-Quijano, F. A.; Kovacs, Z.; Sherry, D. *Inorg Chem.* **2011**, *50*, 1648−1655.
(6) Roca-Sabio, A.; Bonnet, C. S.; Mato-Iglesias, M.; Esteban-Gomez, D.; Toth, E.; de-Blas, A.; Rodriguez-Blas, A.; Platas-Iglesias, C. *Inorg. Chem.* **2012**, *20*, 10893−10903.
(7) Chandira, S.; Tyagi, M.; Agrawal, S. *J. Serb. Chem. Soc.* **2010**, *7*, 935−941.
(8) Dorazioi, S. J.; Tsitovich, P. B.; Gardina, S. A.; Morrow, J. R. *J. Inorg. Biochem.* **2012**, *117*, 212−219.
(9) Woodin, K. S.; Heroux, K. J.; Boswell, A. C.; Wong, E. H.; Weisman, G. R.; Niu, W.; Tomellini, S. A.; Anderson, C. J.; Zakharov, L. N.; Rheingold, A. L. *Eur. J. Inorg. Chem.* **2005**, *23*, 4829−4833.
(10) Ghachtouli, S. E.; Cadiou, C.; Dechamps-Olivier, I.; Chuburu, F.; Aplincourt, M.; Patinee, V.; Baccon, M. L.; Handel, H.; Roisnel, T. *New. J. Chem.* **2006**, *30*, 392−398.
(11) Koziel, L.; Valdez, C. A.; Baker, S. E.; Lau, E. Y.; Floyd(III), W. C.; Wong, S. E.; Satcher, J. H.; Lightstone, F. C.; Aines, R. D. *Inorg. Chem.* **2012**, *51*, 6803−6812.
(12) Salter, M. H.; Reibenspies, J. H.; Jones, B.; Hancock, R. D. *Inorg. Chem.* **2005**, *44*, 2791−2797.
(13) Ye, W.; Ho, D. M.; Friedle, S.; Palluccio, T. D.; Rybak-Akimova, E. V. *Inorg. Chem.* **2012**, *51*, 5006−5021.
(14) Atuzen, S.; Korth, H. S.; Grott-de, H.; Sustmann, R. *Eur. J. Org. Chem.* **2001**, *16*, 3119−3125.
(15) Bush, D. H. *Acc. Chem. Res.* **1978**, *11*, 392−400.
(16) Srinivasan, S.; Athappan, P. *Transition Met. Chem.* **2001**, *26*, 588−593.
(17) Casitas, A.; Rivas, X. *Chem. Sci.* **2013**, *4*, 2301−2319.
(18) Raffard, N.; Carina, R.; Simaan, J. A.; Sainton, J.; Riviere, E.; Tehertanov, L.; Bourcier, S.; Bouchoux, G.; Delroisse, M.; Banse, F.; Girerd, G. G. *Eur. J. Inorg. Chem.* **2001**, *9*, 2249−2254.
(19) Fabbrizzi, L. *J. C. S. Dalton* **1979**, 1857−1861.
(20) Sabatini, L.; Fabbrizzi, L. *Inorg. Chem.* **1978**, *18*, 438−444.
(21) Domagala, S.; Malecka, J.; Michalowicz, A.; Mames, I.; Kamienski, B.; Wozny, M.; Bilewicz, R.; Daszkiewicz, B. K.; Wozinak, K. *Eur. J. Inorg. Chem.* **2012**, *23*, 3680−3692.
(22) Fritsky, I. O.; Kozlowski, H.; Kanderal, O. M.; Haukka, M.; Kozlowska, J. S.; Kontecka, E. G.; Meyer, F. *Chem. Commun.* **2006**, 4125−4127.
(23) Buttafava, A.; Fabbrizzi, L.; Perotti, A.; Poggi, A.; Poli, G.; Seghi, B. *Inorg. Chem.* **1986**, *25*, 1456−1461.
(24) Kock, W. O.; Kaiser, J. T.; Kruger, H. J. *Chem. Commun.* **1997**, 2237−2238.
(25) Jeyasubramanian, K.; Samath, A. S.; Thamburdi, S.; Murugesan, R.; Ramalingam, S. K. *Transition Met. Chem.* **1995**, *20*, 76−80.
(26) Fabbrizzi, L.; Lari, A.; Poggi, A. *Inorg. Chem.* **1982**, *21*, 2083−2085.
(27) Kim, J. C.; Fettinger, J. C.; Kim, Y. I. *Inorg. Chem. Acta.* **1999**, *286*, 67−73.
(28) Fabbrizzi, L.; Forlini, F.; Perottie, A.; Seghi, B. *Inorg. Chem.* **1984**, *23*, 807−813.
(29) Ciampolini, M.; Fabbrizzi, L.; Licchelli, M.; Perotti, A.; Pezzini, F.; Poggi, A. *Inorg. Chem.* **1986**, *25*, 4131−4135.
(30) Taki, M.; Kawashima, Y.; Sakai, N.; Hirayama, T.; Yamamoto, Y. *Bull. Chem. Soc. Jpn.* **2008**, *5*, 590−597.
(31) Lincoln, K. M.; Richardson, T. E.; Rutter, L.; Gonzalez, P.; Simpkins, J. W.; Green, K. N. *Acs. Chem. Neurosci.* **2012**, *11*, 919−927.
(32) Lincoln, K. M.; Gonzalez, P.; Richardson, T. E.; Julovich, D. A.; Saunders, R.; Simpkins, J. W.; Green, K. N. *Chem. Commun.* **2013**, *49*, 2712−2714.
(33) Alcock, N. W.; Busch, D. H.; Liu, C. Y. Private communication. 2007. CCDC # $[Mn^{III}\mathbf{L1}Cl_2]^+$, 639156, $[Fe^{III}\mathbf{L1}Cl_2]^+$, 693154; $[Cu^{II}\mathbf{L1}Cl]^+$, 639155; $[Zn^{II}\mathbf{L1}Cl]^+$, 628572.
(34) Bencini, A.; Fabbrizzi, L.; Poggi, A. *Inorg. Chem.* **1981**, *20*, 2544−2549.
(35) Martin, L. Y.; Sperati, R. C.; Busch, D. H. *J. Am. Chem. Soc.* **1977**, *99*, 2968−2981.
(36) Barefield, E. K. Ph.D. Thesis, Ohio State University, 1969.
(37) Mochizuki, K.; Sugita, T.; Kuriowa, S.; Yamada, F.; Hayano, K.; Ohgami, Y.; Suzui, M.; Kato, S. *Inorg. Chim. Acta* **2010**, *363*, 3151−3157.
(38) Mochizuki, K.; Fujimoto, M.; Ito, H.; Ito, T. *Bull. Chem. Soc. Jpn.* **1980**, *53*, 2535−2539.
(39) Mochizuki, K.; Ikeda, Y. *Bull. Chem. Soc. Jpn.* **1990**, *63*, 1587−1591.
(40) Pallavicini, P. S.; Perottie, A.; Poggi, A.; Seghi, B.; Fabbrizzi, L. *J. Am. Chem. Soc.* **1987**, *109*, 5139−5144.
(41) Alcock, N. W.; Moore, P.; Omar, H. A. *J. Chem. Soc., Dalton Trans.* **1986**, 985−989.
(42) Lovecchio, F. V.; Gore, E. S.; Busch, D. H. *J. Am. Chem. Soc.* **1974**, *96*, 3109−3118.
(43) Brines, L.; Shearer, J.; Fender, J. K.; Schweitzer, D.; Shoner, S. D.; Barnhart, D.; Kaminsky, W.; Kovacs, J. *Inorg. Chem.* **2007**, *46*, 9267−9277.
(44) Mas, P. L.; Taylor, W.; Schweitzer, D.; Thelsen, R. M.; Xu, L.; Shearer, J.; Swartz, R. D.; Gleaves, M. C.; DiPasquale, A.; Kaminsky, W.; Kovacs, J. *Inorg. Chem.* **2008**, *47*, 11228−11236.
(45) Addsion, A. W.; Rao, N. T. *J. Chem. Soc., Dalton Trans.* **1984**, 1349−1356.
(46) Felix, V.; Costa, J.; Delgado, R.; Drew, M. B.; Duarte, M. T.; Resende, C. *J. Chem. Soc., Dalton Trans.* **2001**, 1462−1471.
(47) Felix, V.; Calhorda, M. J.; Costa, J.; Delgado, R.; Brito, C.; Duarte, M. T.; Arcos, T.; Drew, M. B. *J. Chem. Soc., Dalton Trans.* **1996**, 4543−4553.
(48) Fabbrizzi, L.; Forlini, F.; Perotti, A.; Seghi, B. *Inorg. Chem.* **1984**, *23*, 807−813.
(49) Castellani, C. B; Fabbrizzi, L.; Lichelli, M.; Perotti, A.; Poggi, A. *J. Chem. Soc., Chem. Commun.* **1984**, 806−808.
(50) Fabbrizzi, l.; Poggi, A. *J. Chem. Soc., Chem. Commun.* **1980**, 646−647.
(51) Barefield, K. E.; Busch, D. H. *Chem. Commun.* **1970**, 522−523.
(52) Xifra, R.; Ribas, X.; Llobet, A.; Poater, A.; Duran, M.; Sola, M.; Stack, D. P.; Buchholz-Benet, J.; Donnabieu, B.; Mahia, J.; Parella, T. *Chem.—Eur. J.* **2005**, *11*, 5146−5156.